

# Improving the durability of the optical fiber sensor based on strain transfer analysis



Huaping Wang<sup>a,c</sup>, Lizhong Jiang<sup>a,b</sup>, Ping Xiang<sup>a,b,d,\*</sup>

<sup>a</sup> School of Civil Engineering, Central South University, Changsha 410075, Hunan, China

<sup>b</sup> National Engineering Laboratory for High-speed Railway Construction, Changsha, China

<sup>c</sup> Department of Civil and Environmental Engineering, The Hong Kong Polytechnic University, Hong Kong Special Administrative Region

<sup>d</sup> Department of Architecture and Civil Engineering, City University of Hong Kong, Hong Kong Special Administrative Region

## ARTICLE INFO

### Keywords:

Optical fiber sensor  
Interfacial bonding properties  
Strain transfer analysis  
Interfacial debonding failure  
Error modification  
Application design

## ABSTRACT

To realize the reliable and long-term strain detection, the durability of optical fiber sensors has attracted more and more attention. The packaging technique has been considered as an effective method, which can enhance the survival ratios of optical fiber sensors to resist the harsh construction and service environment in civil engineering. To monitor the internal strain of structures, the embedded installation is adopted. Due to the different material properties between host material and the protective layer, the monitored structure embedded with sensors can be regarded as a typical model containing inclusions. Interfacial characteristic between the sensor and host material exists obviously, and the contacted interface is prone to debonding failure induced by the large interfacial shear stress. To recognize the local interfacial debonding damage and extend the effective life cycle of the embedded sensor, strain transfer analysis of a general three-layered sensing model is conducted to investigate the failure mechanism. The perturbation of the embedded sensor on the local strain field of host material is discussed. Based on the theoretical analysis, the distribution of the interfacial shear stress along the sensing length is characterized and adopted for the diagnosis of local interfacial debonding, and the sensitive parameters influencing the interfacial shear stress are also investigated. The research in this paper explores the interfacial debonding failure mechanism of embedded sensors based on the strain transfer analysis and provides theoretical basis for enhancing the interfacial bonding properties and improving the durability of embedded optical fiber sensors.

## 1. Introduction

The structural safety of civil infrastructures, ocean platforms and aerospace structures has received increasing attention, because the failure of those important structures usually leads to large abundant of casualties and economical loss. To characterize the structural performance, structural health monitoring (SHM) technology has been recognized as one of the most effective and intelligent measures [18,19,1,23,22,10,7]. By the use of smart sensors and components, the real-time, long-term and continuous information of the in-situ structures can be provided for the damage identification, disaster forecasting and warning, and safety and life-time assessment [35,17,20,16,26]. Among these smart sensing elements, optical fiber based sensors are the most popular in civil engineering for the unique advantages of high sensitivity and precision, corrosion resistance, anti-electromagnetic interference, good stability, geometrical shape-versatility, absolute measurement and convenient integration of network [25,34,32,12].

For the brittle material properties of silica fiber, bare optical fiber is weak to resist the shear or torsion force in structural construction and operation. Especially for the embedded case, the packaging technique is the most critical factor to guarantee the survival and enhance the durability of optical fiber based sensors. However, the existence of the protective layer introduces the intermedium between the sensing fiber and the monitored structure, which makes the strain measured by the sensor not entirely represent the actual strain of host material [2]. The error between the measured strain and the actual strain is attributed to the strain loss in the transferring path. To eliminate the strain transfer error and improve the measurement accuracy of optical fiber based sensors, strain transfer theory has been developed to establish the quantitative relationship of strains between the host material and the optical fiber [13,33,9,28].

Considerable attempts have contributed to studying the strain transfer mechanism of optical fiber sensors. The earliest research started from the 1990s, and the strain relationship between the

\* Corresponding author at: School of Civil Engineering, Central South University, Changsha 410075, Hunan, China.  
E-mail addresses: [pxiang2-c@my.cityu.edu.hk](mailto:pxiang2-c@my.cityu.edu.hk), [pxiang@csu.edu.cn](mailto:pxiang@csu.edu.cn) (P. Xiang).



**Fig. 1.** The optical fiber based sensors used in practical engineering: (a) Steel packaged FBG sensor developed by HBM; (b) GFRP packaged FBG sensor developed by SCAIME; (c) Stainless steel packaged FBG sensor developed by MOI (d) CFRP/GFRP packaged FBG sensor developed by TELL.

concrete and sensing fiber was studied with a polymer-to-glass modulus ratio of 1/200 given [21]. Host material with optical fiber sensor embedded was then simplified to infinite elastic cylinder model, and plane-strain theory was adopted to explore the strain transfer mechanism [24]. However, the simplified model in the two theories couldn't be used to accurately determine the strain transfer relationships for various host materials with non-elastic behavior. In 1998, a systematic strain transfer theory of a three-layered structure embedded with optical fiber sensor was established [3]. To analyze the effects of a local interfacial slippage on the strain transfer ratio, a two-layered mechanical model consisted of host material and optical fiber was discussed [13]. For a multi-layered structure with various packaging layers, the unified strain transfer formula was conducted [33]. The improved strain transfer deduction of a three (multi)-layered sensing model by the use of simplified geometrical and physical functions was proposed [15]. Strain transfer analysis was also extended to special cases for considering the viscoelastic material properties of the monitored structure [30]. For surface-attached point optical fiber sensors, the strain transfer mechanism and sensitivity of influencing parameters was studied [27]. The strain transfer of surface-attached distributed optical fiber sensors with one crack in host material was explored [6]. Besides, the dynamic strain transfer relationship of the sensing model under fatigue load was investigated [31]. In general, most of the existing strain transfer theory mentioned above is based on the non-destructive models, and limit consideration focuses on the damaged model. Besides, the current studies are confined to the strain transfer error modification. The strain transfer theory has yet been adopted to explore the failure mechanism and application design of optical fiber based sensors.

In practical engineering, the premature failure of optical fiber based sensors becomes a common phenomenon. Many installed sensors are out of service in 5 years, the life cycle of which is quite shorter than that of the monitored structure. For embedded cases, it is usually difficult for rehabilitation or replacement, which threatens the real-time performance monitoring of on-site structures. Therefore, the durability and long-term performance of optical fiber based sensors draws considerable attention [29]. When the rehabilitation is not so convenient and the sensor is claimed to work normally, strain transfer error modification with the damaged cases considered becomes particularly significant. The interfacial debonding between the embedded sensor and host material is one of the most common failure modes that should be carefully studied, for it associates with the reliable use and measurement accuracy of optical fiber sensors in practical application. If the local interfacial debonding exists in the embedded sensing model, the strain transfer error modification is also demanded to ensure the

effective measurement. For this reason, the interfacial damage identification and measurement accuracy requires further investigation through the strain transfer analysis between the packaged sensor and host material.

Given the analysis above, the possible failure modes of optical fiber sensors available in the market for the embedment in structures are discussed by considering the strain transfer mechanism. Analysis on the influence of local interfacial debonding between the embedded sensor and host material is studied theoretically. The perturbation of the embedded sensor on the strain field of the structure is discussed. Based on the strain transfer analysis, theoretical approach to diagnose the occurrence of interfacial debonding and debonding length is proposed. Furthermore, the sensitive parameters influencing the interfacial bonding properties are discussed and suggestions on the application design of embedded sensors are provided for improving the durability of the sensor.

## 2. Optical fiber based sensors with enhanced performance

The optical fiber based sensors have been prevailed for decades, and optical fiber has been packaged with various materials to enhance the performance and the robustness of the sensors in practical engineering. Available sensors used for the inside strain detection of concrete (or composite) structures in market majorly contains the following four types presented in Fig. 1, which are separately developed by four internationally famous companies. Steel, glass fiber reinforced plastic (GFRP), carbon fiber reinforced plastic (CFRP) and stainless steel have been separately used as the packaging materials to protect the sensing fiber. It can be noted that the strain of the structure is majorly transferred to the sensor by interfacial shear force. Therefore, the interfacial bonding strength is particularly important to guarantee an effective measurement. Besides of the embedded FBG sensor provided by HBM, the surface of the other three sensors separately developed by SCAIME, MOI and TELL have been polished to increase the roughness. This measure partially improves the interfacial bonding state and finally benefits the long-term effective measurement of the embedded sensors. However, how to quantitatively assess the interfacial bonding strength and scientifically enhance the roughness of the packaged sensor still requires reliable theoretical investigation. For this reason, the strain transfer theory is adopted to explore the interfacial failure mechanism of the three-layered sensing model.

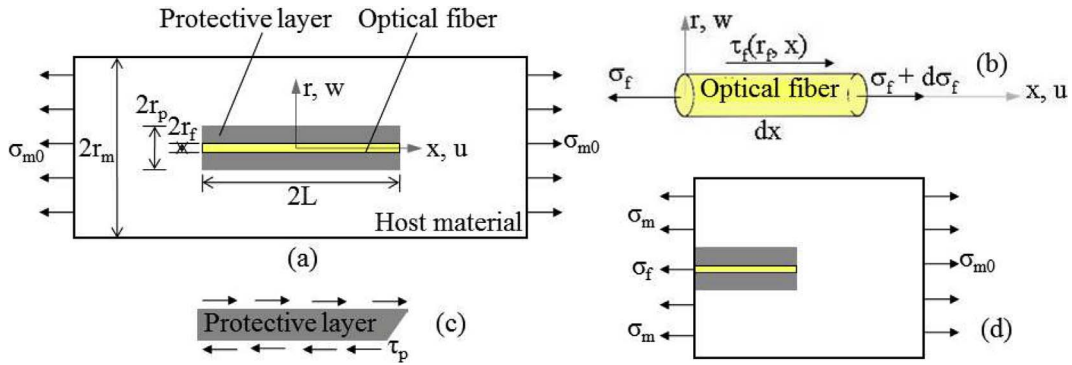


Fig. 2. Optical fiber sensor embedded in structure: (a) Testing model; (b) Stress state of optical fiber; (c) Stress state of protective layer; (d) Stress state of the model.

### 3. Strain transfer analysis

#### 3.1. Model description

In order to obtain the internal strain of concretes, composite structures and multi-layered pavements, optical fiber based sensors are usually required to be embedded and the protective layer is implemented to guarantee the survival. For this reason, the typical optical fiber sensing model is usually composed of host material, protective layer and optical fiber, as shown in Fig. 2(a). The optical fiber used in sensing field is often constituted of fiber core, cladding and coating. The materials of fiber core and cladding are both silicon dioxides, and that of the coating is organic polymer. The three layers jointly bear the deformation induced by external action. The interfacial debonding between the fiber core, cladding and coating is not desired in practical testing [14]. Otherwise, the brittle fiber core is very vulnerable to breakage, which leads to the failure of the measurement. Some published researches stated that the coating absorbs a small part of strain and induces the strain transfer error [3,15]. However, compared with the practical engineering scale, the thickness of the coating (62.5 μm) is extremely small, and the induced measurement error can be neglected. Therefore, the optical fiber is considered as one layer in the theoretical model, with radius equal to 125 μm [31].

The embedded sensor accompanied with host material bears the external effect. When local interfacial shear stress is up to the critical shear strength, the interface is possible to suffer from local debonding. For the embedded case, the local interfacial debonding between the sensor and the host material is difficult to be repaired, which can induce strain transfer loss and influence the measurement accuracy [28]. In practical situation, the embedded sensor is required to continuously monitor the strain of the monitored structure. To accurately interpret the true information of the structure, it is particularly important to diagnose whether the local interfacial debonding between the embedded sensor and the host material occurs. Therefore, study on strain transfer mechanism of the embedded sensing model is significant, which can be adopted to identify the debonding damage and explore the influence of local interfacial debonding on the strain transfer error-modification principle. The work conducted in this section aims to provide a corresponding error modification formula for the high-precision and long-term strain detection of the embedded sensors in the whole life cycle.

Before the theoretical analysis, the following assumptions are made: (1) the deformation of host material is transferred to the sensing fiber by the contacted interfaces; (2) the disturbing of packaged optical fiber sensor on the far-end stress field of host material is ignored. The three-layered structure is affected by tensile stress  $\sigma_{m0}$  from far end. The radiuses of optical fiber, protective layer and host material are  $r_f$ ,  $r_p$  and  $r_m$ , respectively. Sensing length of the sensor is  $2L$ .

#### 3.2. Theoretical derivation

As shown in Fig. 2(b), the equilibrium of optical fiber sensing layer gives

$$\frac{d\sigma_f(x)}{dx} \cdot \frac{r_f}{2} + \tau_f(r_f, x) = 0 \quad (1)$$

where axial stress of optical fiber is independent with variables  $r$  and  $\theta$ . As the slenderness ratio of optical fiber is large, the inner transverse interaction can be ignored and the assumption is reasonable [4].

Equilibrium equation can be established by considering the shearing action of the protective layer

$$\int_0^{2\pi} \tau_f(r_f, x) r_f d\theta dx = \int_0^{2\pi} \tau_p(r_p, x) r_p d\theta dx. \quad (2)$$

Since normal stress of the sensing fiber,  $\sigma_f$ , is independent of  $\theta$ , both the shear stresses  $\tau_f$  and  $\tau_p$  are independent of  $\theta$  on the basis of Eq. (1). Then, Eq. (2) can be simplified as

$$\tau_f(r_f, x) = \frac{r_p}{r_f} \cdot \tau_p(r_p, x) \quad (3)$$

where  $\tau_p(r_p, x)$  is the interfacial shear stress between the protective layer and host material.

A part of the monitored structure is selected, as shown in Fig. 2(d). From the overall equilibrium along the axis  $x$  direction, it can be known that

$$\sigma_f(x) \cdot r_f^2 + \sigma_m \cdot (r_m^2 - r_p^2) = \sigma_{m0} \cdot r_m^2. \quad (4)$$

Because the shear strain of protective layer,  $\gamma_p(x)$ , is determined by displacements of optical fiber and host material [4,11], an equation can be generated

$$u_m(x) - u_f(x) = \gamma_p(x) (r_p - r_f). \quad (5)$$

By adopting the geometrical and physical equations, and taking the derivation of Eq. (5) with respect to  $x$ , we can obtain

$$\varepsilon_m - \varepsilon_f(x) = \frac{(r_p - r_f)}{G_p} \cdot \frac{d\tau_p(r_p, x)}{dx}. \quad (6)$$

Taking the derivation of Eq. (1) with respect to  $x$ , and replacing  $d\tau_f(r_f, x)/dx$  by Eqs. (1) and (6) can be further expressed as

$$\frac{E_f r_f (r_p - r_f)}{2G_p} \cdot \frac{d^2 \varepsilon_f(x)}{dx^2} - \varepsilon_f(x) = -\frac{\sigma_m}{E_m}. \quad (7)$$

By using Eq. (4), the stress of host material,  $\sigma_m$ , can be replaced by far-end stress of host material,  $\sigma_{m0}$ , and then Eq. (7) can be rewritten as

$$\frac{d^2 \varepsilon_f(x)}{dx^2} - \lambda_1^2 \cdot \varepsilon_f(x) = -\lambda_0^2 \frac{\sigma_{m0}}{E_m} \quad (8)$$

where  $\sigma_{m0}/E_m$  is the far-end strain of host material and denoted as  $\varepsilon_{m0}$ , constants  $\lambda_1$  and  $\lambda_0$  are used to replace the constant terms and expressed

as

$$\lambda_1^2 = \frac{2G_p}{E_f r_f (r_p - r_f)} \left[ 1 + \frac{E_f r_f^2}{E_m (r_m^2 - r_p^2)} \right], \quad \lambda_0^2 = \frac{2G_p r_m^2}{E_f r_f (r_p - r_f) (r_m^2 - r_p^2)}. \quad (9)$$

The general solution of Eq. (8) can be given by

$$\varepsilon_f(x) = A \sinh(\lambda_1 x) + B \cosh(\lambda_1 x) + \frac{\lambda_0^2}{\lambda_1^2} \varepsilon_{m0}. \quad (10)$$

Since no axial force or constraint is applied on the two ends of optical fiber, the axial stresses at  $x = \pm L$  are zero. According to the Hooke's law, the strain of optical fiber at the two ends can be known as

$$\varepsilon_f(\pm L) = 0. \quad (11)$$

By substituting Eq. (11) into Eq. (10), the relationship between the strain of optical fiber and the far-end strain of host material can be expressed as

$$\varepsilon_f(x) = \varepsilon_{m0} \cdot \frac{\lambda_0^2}{\lambda_1^2} \left[ 1 - \frac{\cosh(\lambda_1 x)}{\cosh(\lambda_1 L)} \right] \quad (12)$$

where Eq. (12) explains the strain transfer relationship of the three-layered sensing model at nondestructive stage.

To inspect the accuracy of the proposed strain transfer function, quantitative comparison is required. Values of correlated parameters included in Eq. (12) follow Table 1. Comparison with representative research from Ansari and Yuan [3] is displayed in Fig. 3. General trend of the two curves is that strain transfer ratio decreases from symmetric center to the ends, which declares the correctness and availability of the proposed strain transfer function in this article. Strain transfer ratio at the center (origin of abscissa axis in Fig. 3) is about 98.7%. For the existence of the protective layer, strain of host material cannot be totally delivered to the optical fiber. That is to say, strain transfer coefficient  $\beta$  at the center ( $x = 0$ ) should be smaller than 1, which makes this result approval.

#### 4. Strain perturbation induced by the embedment of optical fiber sensor

The analysis provided in this section can be used to consider the perturbation of the embedded sensor on strain field of the monitored structure and instruct the design on the protective thickness of the sensor in practical engineering. General solution of Eq. (7) with two strain variables of optical fiber and host material around the sensor can be obtained and further solved by considering boundary condition Eq. (11):

$$\varepsilon_f(x) = \varepsilon_m \cdot \left[ 1 - \frac{\cosh(\lambda_2 x)}{\cosh(\lambda_2 L)} \right] \quad (13)$$

where  $\lambda_2^2 = \frac{2G_p}{E_f r_f (r_p - r_f)}$ .

Eq. (13) indicates the strain relationship between optical fiber and host material around the embedded sensor. By comparing Eq. (12) with Eq. (13), the influence of embedded optical fiber sensors on the disturbance of local strain field of the monitored structure can be inspected. Substituting the correlated parameters in Table 1 into Eqs. (12)

**Table 1**  
Material and geometrical parameters of the three-layered sensing model.

Mechanical title	Label	Value	Unit
Young's modulus of optical fiber	$E_f$	$7.2 \times 10^{10}$	N/m <sup>2</sup>
Radius of optical fiber	$r_f$	$1.25 \times 10^{-4}$	m
Shear modulus of the protective layer	$G_p$	$2.25 \times 10^6$	N/m <sup>2</sup>
Out radius of the protective layer	$r_p$	$2.5 \times 10^{-4}$	m
Young's modulus of host material	$E_m$	$2.2 \times 10^9$	N/m <sup>2</sup>
Radius of host material	$r_m$	0.05	m
Half of the bonded length	$L$	0.04	m

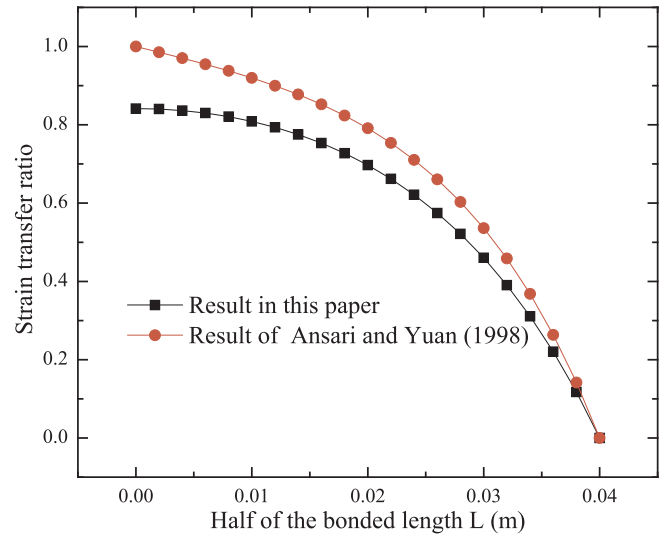


Fig. 3. Strain transfer ratio along half of the bonded length.

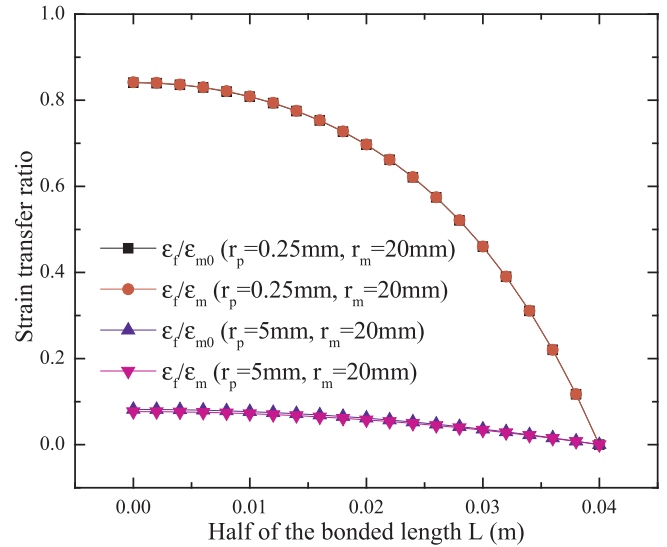


Fig. 4. Strain transfer ratios of  $\varepsilon_f/\varepsilon_m$  and  $\varepsilon_f/\varepsilon_{m0}$  at different radiuses of the protective layer.

and (13), the ratios of  $\varepsilon_f/\varepsilon_m$  and  $\varepsilon_f/\varepsilon_{m0}$  are calculated out, as displayed in Fig. 4. Good overlapping of the two curves is observed, which demonstrates that the embedded sensing fiber with protective layer ( $r_p = 0.25$  mm) has little influence on the strain distribution of the structure.

However, to ensure the survival of the embedded sensor in civil engineering, the out radius of the protective layer can be up to 5 mm. In this case, the influence of the sensor on the strain field of the monitored structure (as shown in Fig. 4) cannot be ignored, and using Eq. (12) can much accurately reflect the actual strain of the host material. It also should be noted that the low strain transfer ratio induced by the thick protective coatings means the strain measured by the optical fiber sensor quite smaller than that of the host material for the high strain loss in the transferring path. In other words, the optical sensing element should be very sensitive to the variation of the micro strain, and then FBG sensor with wavelength resolution up to 1 pm can be adopted in this case. Besides, in practical application, the embedded sensor should have ignorable influence on the structural integrity. Therefore, the thickness of the protective layer is limited in an appropriate range.

### 5. Influence of local interfacial debonding on the strain transfer ratio

For the embedded case, the sensor and the host material will jointly bear the external force. After working for a much long time or suffering from sudden large deformation, the interface between the sensor and host material is possible to be locally damaged, and it may weaken the sensing performance of the sensor and lead to the failure of the testing. To implement the effective measurement, the local interfacial debonding need to be diagnosed and the influence of local interfacial debonding between the sensor and host material on the strain transfer ratio is discussed.

When the interfacial stress between host material and the protective layer reaches the critical state, local interfacial debonding may occur. Thus, the effect of shear force should be taken into consideration. By substituting Eq. (12) into Eq. (1), the shear stress  $\tau_p(r_p, x)$  can be incorporated with Eq. (3), and further expressed as

$$\tau_p(r_p, x) = \frac{E_f r_f^2 \lambda_0^2 \sigma_{m0} \sinh(\lambda_1 x)}{2r_p \lambda_1 E_m \cosh(\lambda_1 L)} \quad (14)$$

By utilizing data from Table 1 and Eq. (14), distribution of the ratio of shear stress to far-end stress along half of the bonded length can be obtained as shown in Fig. 5. The shear stress shows a nonlinear increase by approaching to the end. That is to say, the debonding damage often begins from the end. In the proposed model, the maximum shear stress located at the bonded-length end and the value is  $\tau_p = 0.064\sigma_{m0}$ . Critical interfacial shear stress between host material and the protective layer can be represented as  $\tau_{pcr}$ , which is usually a constant. When the materials of the monitored structure and protective layer are selected [14,8], it can be further determined by experiments.

When  $\tau_p|_{x=L} < \tau_{pcr}$ , no debonding appears in the interface and Eq. (12) can be used to modify the strain transfer error of the sensing model. Otherwise if  $\tau_p|_{x=L} \geq \tau_{pcr}$ , local debonding will occur in the interface between the host material and the sensor [5]. By using Eq. (14), the critical debonding point  $L_d$  is solved out

$$\sinh(\lambda_1 L_d) = \frac{2r_p \lambda_1 E_m \tau_{pcr} \cosh(\lambda_1 L)}{r_f^2 \lambda_0^2 E_f \sigma_{m0}} \quad (15)$$

where  $L_d$  is the debonding point when the host material is subjected to the action of the far-end stress  $\sigma_{m0}$ . At this state, the effective sensing length is  $L_d$ , and the debonding length is  $L-L_d$ , as shown in Fig. 6. Boundary conditions are changed in comparison with no-debonding status, which gives

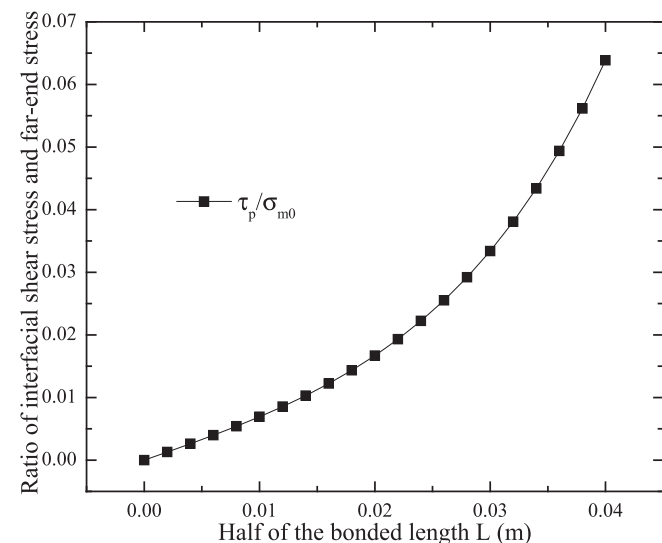


Fig. 5. Ratio of interfacial shear stress and remote stress along half of the bonded length.

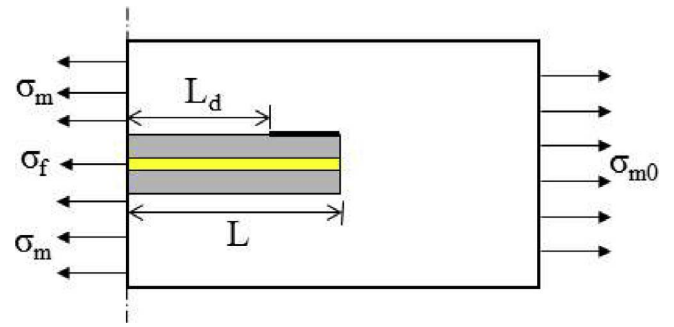


Fig. 6. The interfacial debonding between host material and the protective layer.

$$\varepsilon_f(-L + L_d) = \varepsilon_f(L-L_d) = 0. \quad (16)$$

Substituting Eq. (16) into Eq. (10), the relationship between the strain of optical fiber and far-end strain of host material can be expressed as

$$\varepsilon_f(x) = \varepsilon_{m0} \frac{\lambda_0^2}{\lambda_1^2} \left[ 1 - \frac{\cosh(\lambda_1 x)}{\cosh(\lambda_1 L_d)} \right] \quad (17)$$

where Eq. (17) is the strain transfer error correction formula with the influence of local interfacial debonding considered. In the proposed model, if the maximum interfacial shear stress between host material and the sensor is 0.05 times of the far-end normal stress, namely  $\tau_{pcr} = 0.05\sigma_{m0}$ , the critical effective bonded length can be calculated by using Eq. (15) as  $L_d = 0.036$  m. Substituting  $L_d$  to Eq. (17), the strain transfer ratio can be figured out and the variation along the bonded length is displayed in Fig. 7.

It can be seen that the local debonding brings about the decrease of strain transfer efficiency, and the strain transfer ratio will drop significantly with the increase of the debonding length. Therefore, it is important to prevent the local debonding at the interface between the packaged sensor and the host material.

### 6. Parametric studies

Given the analysis above, it can be noted that the interfacial shear stress determines whether the local debonding damage occurs. Therefore, to effectively control the interfacial bonding state between the sensor and the host material, and ensure the reliable detection of optical fiber sensors embedded in civil structures, the correlated material and geometrical parameters that influence the interfacial shear

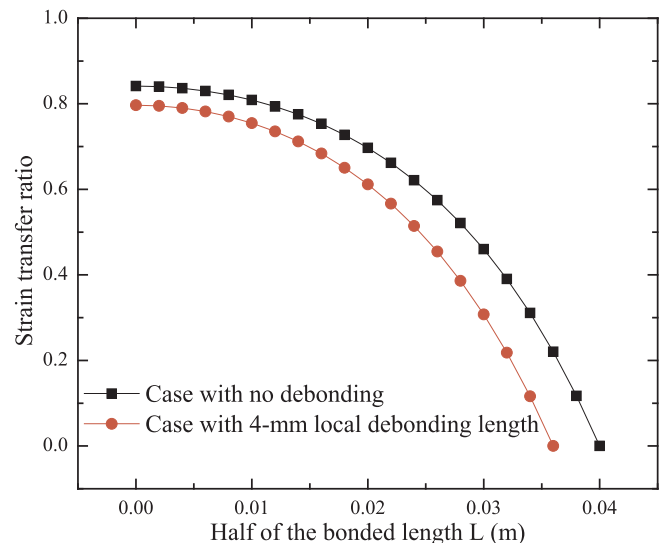


Fig. 7. Comparison of strain transfer ratios with and without local interfacial debonding.

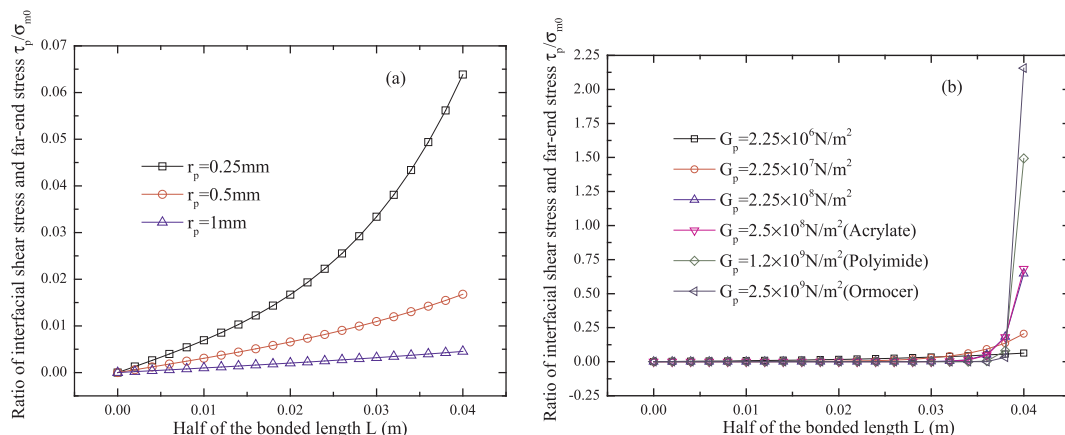


Fig. 8. Influence of material and geometrical parameters of the protective layer on the interfacial shear stress: (a) Radius; (b) Shear modulus.

stress should be carefully discussed, so to understand the interfacial mechanical action. Since the properties of optical fiber are constant, the parametric studies focus on that of the protective layer and host material. The sensitivity analysis is based on the case with parameters listed in Table 1.

6.1. Effect of radius and shear modulus of the protective layer on the interfacial shear stress

Fig. 8(a) shows the ratio of interfacial shear stress  $\tau_p$  and far-end stress  $\sigma_{m0}$  decreased with the increase of radius of the protective layer. The ratio  $\tau_p/\sigma_{m0}$  at the end of the bonded length varies from 0.064, 0.017 to 0.004, with the radius of the protective layer changed from 0.25 mm, 0.5 mm to 1 mm. A significant decrease of the interfacial shear stress is observed with  $r_p$  increased from 0.25 mm to 0.5 mm. Generally, it indicates that the thinner protective layer can bring about larger interfacial shear stress. To prevent the local interfacial debonding, the interfacial shear stress should be as smaller as possible. Therefore, it is important to relatively increase the thickness of the protective layer, since the thicker protective layer may induce larger strain transfer error.

Fig. 8(b) demonstrates the evolution of the ratio of interfacial shear stress and far-end stress with the increase of shear modulus of the protective layer. The protective material discussed in the model is hyper-elastic silicone rubber, with a shear modulus of  $2.25 \times 10^6$  N/m<sup>2</sup>. The silicone rubber is a kind of flexible transparent adhesive with good elasticity, which has been widely used as coating material and substrate. Since acrylate, polyimide and ormocer can also be used as the protective coatings of the sensing fiber, the case study on the

distribution of the interfacial shear stress along the bonded length with  $G_p$  increased separately from  $2.5 \times 10^8$  N/m<sup>2</sup> (acrylate),  $1.2 \times 10^9$  N/m<sup>2</sup> (polyimide) to  $2.5 \times 10^9$  N/m<sup>2</sup> (ormocer) has been investigated. When  $G_p$  varied from  $2.25 \times 10^7$  N/m<sup>2</sup> to  $2.25 \times 10^8$  N/m<sup>2</sup>, the interfacial shear stress approaching the bonded-length end experiences a large increase, with value varied from  $0.2\sigma_{m0}$  to  $0.65\sigma_{m0}$ , which may lead to end interfacial debonding. Although the higher shear modulus of the protective coating can bring about a smaller interfacial shear stresses in the bonded-length range of 0–0.035 m, the interfacial shear stress at the end of the boned length is quite larger, which can easily induce interfacial end debonding. A comprehensive consideration is required to reasonably select the protective material to guarantee the distributed interfacial shear stresses along the bonded length in much low level. In general, it is better to select flexible protective material with relatively high bonding performance. To prevent the occurrence of local interfacial debonding, the shear modulus of the protective layer is suggested to be around  $2.25 \times 10^7$  N/m<sup>2</sup> for the proposed model. For example, the high- or low-density polyethylene with the shear modulus approaching the suggested values can be selected as the protective material for the sensing fiber.

6.2. Effect of radius and Young’s modulus of host material on the interfacial shear stress

The well-overlapped curves in Fig. 9(a) demonstrate that the change of radius of host material has ignorable influence on the interfacial shear stress. Therefore, other parameters should be particularly considered in the design of the embedded sensor, so as to decrease the risk of the local interfacial debonding. Fig. 9(b) illustrates that the higher

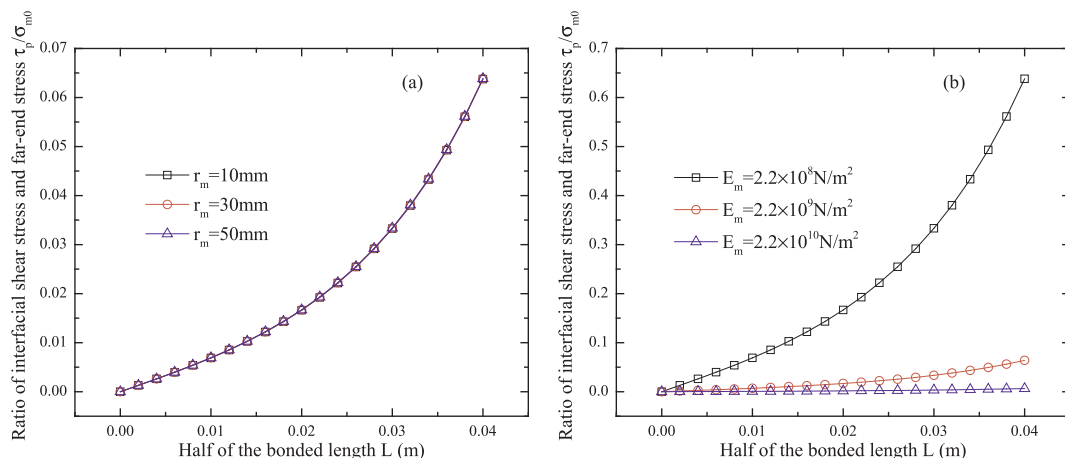


Fig. 9. Influence of material and geometrical parameters of the host material on the interfacial shear stress: (a) Radius; (b) Young’s modulus.

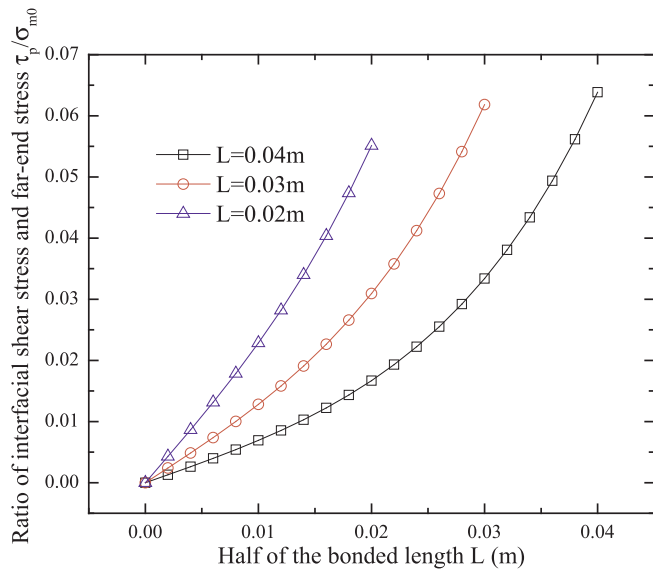


Fig. 10. Influence of bonded length on the interfacial shear stress.

Young's modulus of host material brings about smaller interfacial shear stress. When  $E_m$  changes from  $2.2 \times 10^8 \text{ N/m}^2$  to  $2.2 \times 10^9 \text{ N/m}^2$ , a sharp decrease is noticed, and the decreasing amplitude becomes smooth with  $E_m$  increased from  $2.2 \times 10^9 \text{ N/m}^2$  to  $2.2 \times 10^{10} \text{ N/m}^2$ . This conclusion indicates that when the sensor is employed to detect the strain of host material with low modulus, the interfacial debonding should be particularly considered.

### 6.3. Effect of bonded length on the interfacial shear stress

Fig. 10 shows the evolution of interfacial shear stress with the variation of the bonded length. Generally speaking, the longer bonded length brings about relatively larger interfacial shear stress. When  $L$  increases from 0.02 m to 0.04 m, the interfacial shear stress at the bonded-length end goes through a slow growth, and the maximum value increases from  $0.055\sigma_{m0}$  to  $0.063\sigma_{m0}$ . When half of the bonded length increases from 0.03 m to 0.04 m, the growth of the maximum interfacial shear stress becomes smooth. It means that the bonded length has relatively small influence on the maximum amplitude of the interfacial shear stresses. The increasing gradients of the three curves in Fig. 10 indicate that the shorter bonded length can bring about a sharper growth of the interfacial shear stresses. That is to say, the larger normal stress of the host material can lead to higher interfacial shear stresses in the bonded-length interval, and local interfacial debonding damage is prone to occurrence. The increasing gradients become gradual with the growth of  $L$  from 0.02 m to 0.04 m. Therefore, in practical engineering, it is better to select relatively long bonded length to delay the occurrence of the local interfacial debonding when the other requirements are satisfied. For the given model,  $L$  equal to 0.03 m can be the best choice.

## 7. Conclusions

It is well known that the uncoordinated deformation induced by the mismatch of material properties of each layer in a multi-layered structure is prone to interfacial debonding failure between the adjacent layers under the external loading. For the commonly used sensing model, the interface between the monitored structure and the embedded sensor is also vulnerable to interfacial damage. To enhance the interfacial bonding properties and guarantee the relatively long-term effective measurement, theoretical approach based on the strain transfer analysis is performed and the following conclusions can be drawn from the study:

- (1) The perturbation of the embedded sensor on the strain field of the host material can be assessed by the overlapped degree of Eqs. (12) and (13), which can be used to determine the maximum radius of the protective layer.
- (2) Eq. (14) can be used to diagnose the occurrence of local interfacial debonding between the sensor and host material, and the related strain transfer error modification of the model with influence of local interfacial debonding considered follows Eq. (17). The local interfacial debonding decreases the strain transfer ratio and enough interfacial bonding strength should be guaranteed, especially at the bonded-length ends of the multi-layered sensing model.
- (3) To prevent the local interfacial debonding between the embedded sensor and host material and enhance the effective measurement of the sensor, the thicker protective layer with relatively lower modulus and the longer gauge length are suggested in the application design. When the embedded sensor is employed to detect the strain of host material with low modulus, the interfacial debonding should be carefully considered by the proposed strain transfer theory.

## Acknowledgements

The writers are greatly appreciating for editors and referees spending time in attentively reading and checking this article. This work is supported by National Science and Technology Support Project (Grant No. 2011BAK02B01), State 863 Project (Grant No. 2014AA110401) and Key Laboratory Scientific Research Special Topics (No. DUT1LAB03). Special thanks are given to Prof. Zhi Zhou and Prof. Jinping Ou of Dalian University of Technology. The findings and opinions expressed in this article are only those of the authors and do not necessarily reflect the views of the sponsors.

## References

- [1] F. Ansari, *Sensing Issues in Civil Structural Health Monitoring*, Springer, Dordrecht, The Netherlands, 2005.
- [2] F. Ansari, Practical implement of optical fiber sensors in civil structural health monitoring of bridges, *J Intell Mater Syst Struct* 18 (8) (2007) 879–889, <http://dx.doi.org/10.1177/1045389X06075760>.
- [3] F. Ansari, L.B. Yuan, Mechanics of bond and interface shear transfer in optical fiber sensors, *J Eng Mech* 4 (1998) 385–394, [http://dx.doi.org/10.1061/\(ASCE\)0733-9399\(1998\)124:4\(385\)](http://dx.doi.org/10.1061/(ASCE)0733-9399(1998)124:4(385)).
- [4] C.T. Chon, C.T. Sun, Stress distributions along a short fibre in fibre reinforced plastics, *J. Mater. Sci.* 15 (1980) 931–938, <http://dx.doi.org/10.1007/BF00552105>.
- [5] J.G. Dai, W.Y. Gao, J.G. Teng, Bond-slip model for frp laminates externally bonded to concrete at elevated temperature, *J Compos Constr* 17 (2) (2013) 217–228, [http://dx.doi.org/10.1061/\(ASCE\)CC.1943-5614.0000337](http://dx.doi.org/10.1061/(ASCE)CC.1943-5614.0000337).
- [6] X. Feng, J. Zhou, C.S. Sun, X.T. Zhang, F. Ansari, Theoretical and experimental investigation into crack detection with BOTDA distributed fiber optic sensors, *J Eng Mech* 139 (12) (2013) 1797–1807, [http://dx.doi.org/10.1061/\(ASCE\)EM.1943-7889.0000622](http://dx.doi.org/10.1061/(ASCE)EM.1943-7889.0000622).
- [7] D.M. Frangopol, M. Soliman, Life cycle of structural systems: recent achievements and future directions, *Struct Infrastruct Eng* 12 (1) (2016) 1–20, <http://dx.doi.org/10.1080/15732479.2014.999794>.
- [8] W.Y. Gao, J.G. Dai, J.G. Teng, Analysis of mode II debonding behavior of fiber-reinforced polymer-to-substrate bonded joints subjected to combined thermal and mechanical loading, *Eng Fract Mech* 136 (2015) 241–264, <http://dx.doi.org/10.1016/j.engfracmech.2015.02.002>.
- [9] B. Glisic, Influence of the gauge length on the accuracy of long-gauge sensors employed in monitoring of prismatic beams, *Meas Sci Technol* 22 (3) (2011) 5206, <http://dx.doi.org/10.1088/0957-0233/22/3/035206>.
- [10] B. Glisic, Y. Yao, Fiber optic method for health assessment of pipelines subjected to earthquake-induced ground movement, *Struct. Health Monit.* 11 (6) (2012) 696–711, <http://dx.doi.org/10.1177/1475921712455683>.
- [11] S.C. Her, C.Y. Huang, Effect of coating on the strain transfer of optical fiber sensors, *Sensors* 11 (7) (2011) 6926–6941, <http://dx.doi.org/10.3390/s110706926>.
- [12] D. Kinet, P. Megret, K.W. Goossen, L. Qiu, D. Heider, C. Caucheteur, Fiber Bragg grating sensors toward structural health monitoring in composites materials: challenges and solutions, *Sensors* 14 (2014) 7394–7419.
- [13] M. LeBlanc, *Interaction mechanics of embedded single-ended optical fibre sensors using novel in-situ measurement Techniques*, University of Toronto, Canada, 1999 (Thesis for the degree of Doctor).
- [14] C.K.Y. Leung, X.Y. Wang, N. Olson, Debonding and calibration shift of optical fiber sensors in concrete, *J Eng Mech* 126 (3) (2000) 300–307, [http://dx.doi.org/10.1061/\(ASCE\)0733-9399\(2000\)126:3\(300\)](http://dx.doi.org/10.1061/(ASCE)0733-9399(2000)126:3(300)).

- [15] H.N. Li, G.D. Zhou, L. Ren, D.S. Li, Strain transfer coefficient analysis for embedded fiber Bragg grating sensors in different host materials, *J Eng Mech* 135 (12) (2009) 1343–1353, [http://dx.doi.org/10.1061/\(ASCE\)0733-9399\(2009\)135:12\(1343\)](http://dx.doi.org/10.1061/(ASCE)0733-9399(2009)135:12(1343)).
- [16] G. Luyckx, E. Voet, N. Lammens, J. Degrieck, Strain measurements of composite laminates with embedded fibre Bragg gratings: criticism and opportunities for research, *Sensors* 11 (2011) 384–408.
- [17] A. Mufti, Guidelines for Structural Health Monitoring. Design Manual No.2, ISIS Canada, Manitoba, Canada, 2006.
- [18] H. Murayama, K. Kageyama, H. Naruse, A. Shimada, K. Uzawa, Application of fiber-optic distributed sensors to health monitoring for full-scale composite structures, *J Intell Mater Syst Struct* 14 (2003) 3–11.
- [19] H. Murayama, K. Kageyama, T. Kamita, H. Igawa, Structural health monitoring of a full-scale composite structure with fiber-optic sensors, *Adv Compos Mater* 11 (3) (2003) 287–297.
- [20] H. Murayama, K. Kageyama, K. Uzawa, K. Ohara, H. Igawa, Strain monitoring of a single-lap joint with embedded fiber-optic distributed sensors, *Struct. Health Monit.* 11 (3) (2011) 325–344.
- [21] A. Nanni, C.C. Yang, K. Pan, J.S. Wang, R.R.M. Jr, Fiber-optic sensors for concrete strain/stress measurement, *ACI Mater. J.* 88 (3) (1991) 257–264.
- [22] Y.Q. Ni, K.H. Lam, D. Zhu, Y. Wang, J.P. Lynch, K.H. Law, In-construction vibration monitoring of a super-tall structure using a long-range wireless sensing system, *Smart Struct. Syst.* 7 (2011) 83–102.
- [23] J.P. Ou, H. Li, Structural health monitoring in mainland China: review and future trends, *Struct. Health Monit.* 9 (3) (2010) 219–231, <http://dx.doi.org/10.1177/1475921710365269>.
- [24] Y.E. Pak, Longitudinal shear transfer in fiber optic sensors, *Smart Mater Struct* 1 (1992) 57–62, <http://dx.doi.org/10.1088/0964-1726/1/1/008>.
- [25] J.S. Sirkis, Unified approach to phase-strain-temperature models for smart structure interferometric optical fiber sensors: part 2, applications, *Opt Eng* 32 (4) (1993) 762–773, <http://dx.doi.org/10.1117/12.61198>.
- [26] S. Sulejmani, C. Sonnenfeld, T. Geernaert, G. Luyckx, P. Mergo, W. Urbanczyk, K. Chah, H. Thienpont, F. Berghmans, Disbond monitoring in adhesive joints using shear stress optical fiber sensors, *Smart Mater Struct* 23 (2014) 1–10.
- [27] K.T. Wan, C.K.Y. Leung, N.G. Olson, Investigation of the strain transfer for surface-attached optical fiber strain sensors, *Smart Mater Struct* 17 (2008) 0964–1726, <http://dx.doi.org/10.1088/0964-1726/17/3/035037>.
- [28] H.P. Wang, Strain transfer of optical fiber under damage conditions and its application in multi-layered pavements, Dalian University of Technology, Dalian, 2015 (Thesis for Doctoral Degree in Engineering).
- [29] H.P. Wang, L.Z. Jiang, P. Xiang, Priority design parameters of industrialized optical fiber sensors in civil engineering, *Opt Laser Technol* 100 (2018) 119–128.
- [30] H.P. Wang, P. Xiang, Strain transfer analysis of optical fiber based sensors embedded in an asphalt pavement structure, *Meas Sci Technol* 27 (7) (2016) 75106–75117, <http://dx.doi.org/10.1088/0957-0233/27/7/075106>.
- [31] H.P. Wang, P. Xiang, X. Li, Theoretical analysis on strain transfer error of FBG sensors attached on steel structures subjected to fatigue load, *Strain* (2016), <http://dx.doi.org/10.1111/str.12195> in press.
- [32] H.P. Wang, W.Q. Liu, J.P. He, X.Y. Xing, D.D. Cao, X.P. Gao, X.W. Hao, H.W. Chen, Z. Zhou, Functionality enhancement of industrialized optical fiber sensors and system developed for full-scale pavement monitoring, *Sensors* 14 (5) (2014) 8829–8850, <http://dx.doi.org/10.3390/s140508829>.
- [33] Z. Zhou, Optical fiber smart Bragg grating sensors and intelligent monitoring systems of civil infrastructures, Harbin Institute of Technology, Harbin, 2003 (Dissertation for the Doctoral Degree in Engineering).
- [34] Z. Zhou, W.Q. Liu, Y. Huang, H.P. Wang, J.P. He, M.H. Huang, J.P. Ou, Optical fiber Bragg grating sensor assembly for 3D strain monitoring and its case study in highway pavement, *Mech Syst Sig Process* 28 (2012) 36–49, <http://dx.doi.org/10.1016/j.ymssp.2011.10.003>.
- [35] Z. Zhou, J.P. Ou, Development of FBG Sensors for Structural Health Monitoring in Civil Infrastructures. Sensing Issues in Civil Structural Health Monitoring, Springer, 2005 pp. 197–207.